Engineered Science
DOI: https://dx.doi.org/10.30919/es1620

Flow Pattern and Pressure Drop of Two-Phase Air-Water Flow in a Plate Heat Exchanger with Grooved Copper Foam

Kitti Nilpueng[1] and Somchai Wongwises[2,*]

Abstract

This article focuses on the flow patterns and pressure drop of a two-phase air-water mixture in plate heat exchangers (PHEs) that include grooved copper foam inserts. The objective is to advance the design of compact heat exchangers operating under two-phase flow conditions to enhance thermal management and reduce pressure drop. A transparent cover plate is specifically designed to observe flow patterns across a range of gas and liquid superficial velocities ranging from 0.079 to 2.8 m/s and 0.079 to 0.32 m/s, respectively. Visual observations captured by digital and video cameras identify two flow patterns: bubbly flow and churn flow. These flow patterns and their transitions are substantially altered by the insertion of copper foam in PHEs compared to conventional PHEs. Insertion of copper foam in a PHE increases pressure drop. However, this effect can be mitigated by cutting grooves into the copper foam structure. When grooved copper foam is inserted into a PHE (PHE_GCF), the pressure loss is reduced by approximately 48.0% and 59.3% for groove widths of 4 mm and 6 mm, respectively, compared to the pressure drop of a PHE with copper foam (PHE_CF) inserted. New correlations are also created for PHEs, PHE_GCFs, and PHE_CFs to offer practical applications and valuable information for PHE design.

Keywords: Flow pattern; Pressure drop; Two-phase flow; Plate heat exchanger; Grooved copper foam.
Received: 30 March 2025; Revised: 15 May 2025; Accepted: 17 June 2025.
Article type: Research article.

1. Introduction

Plate heat exchangers (PHEs) have been utilized in different applications in a wide range of industrial processes, including petrochemical operations, oil refining, food processing, and cooling systems, amongst others. Their advantages over other heat exchanger types include a high heat transfer coefficient (HTC), compactness, and ease of maintenance. PHEs are primarily utilized for single-phase flow applications. Evaporators and condensers in air conditioning or refrigeration systems are examples of two-phase flow applications that are increasingly used. A two-phase flow pattern significantly impacts the pressure drop (ΔP), heat transfer, and mass transfer during phase transitions. Therefore, it is essential to have a comprehensive understanding of the two-phase flow pattern and its correlations with ΔP and heat transfer properties within the PHE.

In the past, many researchers conducted in-depth studies on the two-phase flow characteristics present within PHEs. For example, Nilpueng and Wongwises[1] investigated the flow characteristics and pressure loss of a two-phase air-water flow in a PHE with chevron angles of 55° and 10°. The researchers analyzed three distinct flow patterns, bubbly, slug, and annular-liquid bridge. The ΔP underwent significant changes when water and air velocities were modified. Grabenstein *et al.*[2] investigated the characteristics of a two-phase flow in a single corrugated gap of a PHE. Three flow regimes were identified, bubbly, film, and slug flow. It was observed that neither homogeneous nor heterogeneous flow models successfully predicted the ΔP for all patterns. The study conducted by Wei *et al.*[3] involved a numerical analysis of the flow of two phases in a vertical narrow rectangular conduit. The researchers identified four easily distinguishable flow patterns, bubbly, slug, churn-turbulent, and annular flow. Annular flow occurred more frequently, while slug and bubbly flows were less common compared to those in a tube. Jiang and Bai[4] conducted a study on the flow patterns and ΔP in a transparent plate passage with a capsule-type structure.

[1]*Department of Power Engineering Technology, College of Industrial Technology, Engineering, King Mongkut's University of Technology North Bangkok, Bangsue, Bangkok, 10800, Thailand*
[2]*Department of Mechanical Engineering, Faculty of Engineering, King Mongkut's University of Technology Thonburi (KMUTT), Bangmod, Bangkok, 10140, Thailand*
**E-mail:* somchai.won@kmutt.ac.th (S. Wongwises)

The researchers examined the patterns of film, plug, and churn flows and then developed a novel correlation to predict the ΔP based on the Reynolds number (Re). Lee *et al.*[5] examined the flow characteristics and arrangements of R-1234ze (E) in a PHE. Their analysis discerned five main flow regimes, categorized according to vapor quality, slug, wavy liquid film, pulsing annular, vapor-preferred route annular, and full annular flows. Additionally, they documented a correlation between the change in pressure and the various observed flow patterns. Buscher[6] examined air and water movement in a see-through channel with a wavy pattern using digital image processing techniques. This approach was appropriate for automated numerical examination of complex two-phase flows, yielding outcomes that closely matched previously published flow pattern maps. Vatani and Ganji[7] conducted a study on the movement of gas and liquid in a rectangular tunnel sloped in an upward direction. The researchers observed slug, churn, and annular-mist flow patterns. They concluded that the impacts occurring upstream had a substantial influence on the interactions between phases and the transfer of momentum. Passoni *et al.*[8] examined the behavior of two-phase flow and ΔP in a chevron-type PHE with no heat exchange occurring. The researchers discovered many flow regimes, including fine-coarse bubbly, Taylor-like bubbly, heterogeneous, partial film, and film flow. They also established new criteria for forecasting transitions between different flow patterns based on their findings.

In the last decade, mini-scale heat exchangers have garnered significant interest due to the growing demand for compact devices, including miniaturized refrigeration systems and cooling systems for electronic applications. To achieve high heat transfer rates within confined spaces, incorporating metal foam is an attractive solution due to its high surface area-to-volume ratio. Consequently, researchers investigated the flow and heat transfer behavior of single-phase and two-phase flows in heat exchangers filled with metal foam. An examination of the mechanics of R410A flow boiling was done by Zhu *et al.*[9] They used horizontal tubes filled with metal foam. The observed flow patterns were annular flow, plug flow, and slug flow. Metal foam significantly impacted annular flow formation, especially at higher pore densities. Abadi *et al.*[10] examined the heat transfer of R245fa under single-phase conditions using PHEs loaded with metal foam. They reported that the HTC increased by up to 5.1 times compared to conventional PHEs. Abadi *et al.*[11] generated flow pattern maps for mini-tubes filled with metal foam using visualization experiments and high-speed imaging. Annular flow was predominant at high vapor quality, whereas intermittent slug flow occurred at lower vapor qualities, as depicted by their maps. They reported a heat transfer enhancement ratio of up to 3.2 and a ΔP ratio of up to 22 when comparing metal-foam-filled tubes to empty tubes. Ahmed *et al.*[12] presented an innovative design consisting of a pipe partially filled with metallic foam having helical grooves. A numerical simulation was done to enhance the thermal and hydraulic performance while simultaneously reducing the required pumping power. They reported that a configuration with four helical grooves and two pitches at Ri = 0.55 increased the Nusselt number (Nu) by 7% and decreased pumping power requirements by 5%. Nilpueng *et al.*[13] did an investigation into the HTC and ΔP in a small PHE filled with copper foam (PHE_CF). Their findings indicated that the HTC exhibited an improvement of approximately 20.23% to 40.28% compared to a conventional PHE. Nilpueng *et al.*[14] studied the HTC of water in a PHE equipped with grooved metal foam. The efficiency of the PHE with grooved copper foam (PHE_GCF) having a groove width of 2 mm, was similar to that of the PHE_CF at a low Re. Chandora *et al.*[15] examined heat transfer thermal efficiency of water in a gasket plate heat exchanger (GPHE) that had been altered by including metal foam. Their research discovered that the Nusselt number and ΔP for the modified GPHE were 1.97 and 1.89 times greater than those of the plain GPHE, respectively.

Numerous researchers have studied two-phase flow inside PHEs, providing information about relationships between flow patterns, ΔP, and the HTC. With increasing demand for mini-scale heat exchangers within the industrial sector, use of metal foam in these devices has been studied by numerous research groups as a potential means of improving heat transfer. Although metal foam considerably enhances the heat transfer rate, it also has a high ΔP penalty. To address this challenge, Nilpueng *et al.*[14] and Ahmed *et al.*[12] presented a new concept of passages containing grooved metal foam. Their results indicated that single-phase pressure drops (ΔP_{SP}) decreased in passages occupied by grooved metal foam, while heat transfer remained similar to that of passages fully occupied by metal foam. This information is valuable for maximizing heat exchanger performance. However, there remains room for further exploration, particularly in the application of grooved metal foam for two-phase flow inside PHEs. The purpose of the current research is to explore the flow patterns and ΔP of air and water within a PHE equipped with grooved copper foam. The grooved metal foam geometry is inspired by the design of square pin fin heat sinks used in electronic cooling. This configuration is intended to reduce pressure drop while enhancing heat transfer compared to non-grooved metal foam. In this work, the superficial gas and liquid velocities (J_G and J_L), as well as the groove size within the metal foam, are systematically varied. Their effects on flow patterns and pressure variations are examined. A comparison of two-phase pressure drop (ΔP_{TP}) between the measured and the predicted data from existing correlations for PHEs and a PHE_CFs is presented. Additionally, new correlations for the ΔP_{TP} in PHEs, PHE_GCFs, and PHE_CFs are generated and proposed.

2. Experimental apparatus and procedure

Fig. 1 illustrates the design and configuration of an

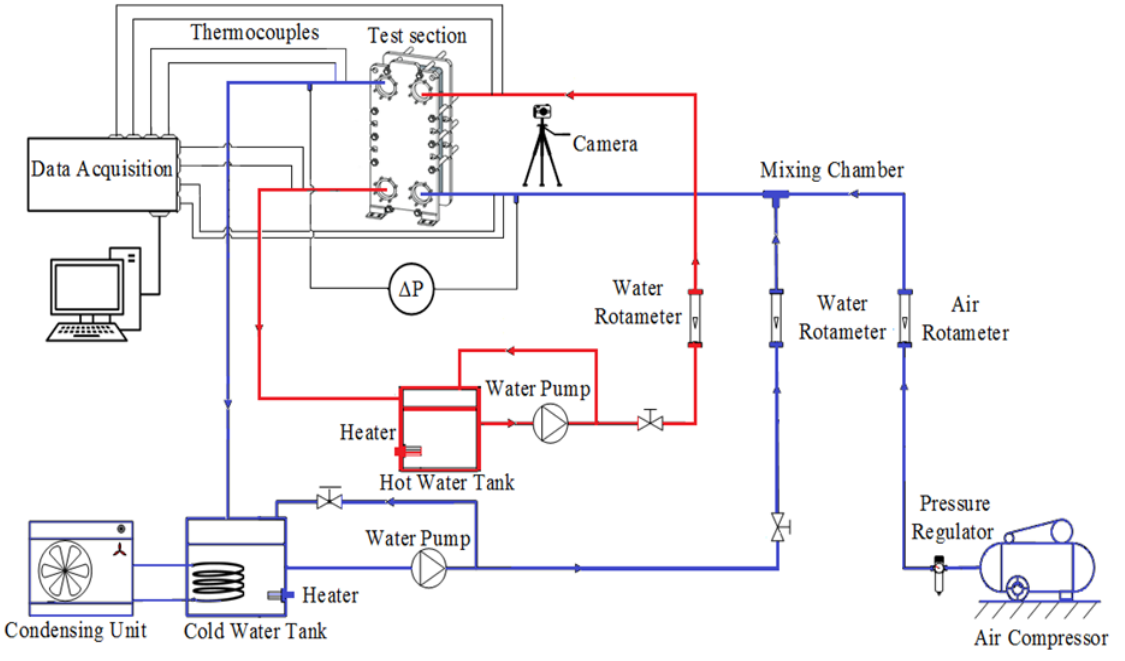

Fig. 1: Schematic diagram of the experimental setup.

experimental apparatus to investigate the flow pattern and ΔP of air and water in a PHE_GCF. A data acquisition system, a test section, and a hot and cold water loop comprised the apparatus. A 3000 W cartridge heater is installed within a 30-liter storage tank in the hot stream loop to regulate the water temperature. A pump is used to transport the hot water from the storage tank to the water rotameter and test section, and then it is returned to the storage tank. A 35-liter storage tank equipped with a 2000 W cartridge heater and a cooling coil connected to a refrigeration system is used to regulate the temperature of the cold water. The cold water in the tank is flowed past the rotameter and PHE, and then returns to the tank. Air from an air compressor passes through an air rotameter and a mixing chamber, where it mixes with cold water before flowing through the test section. Three sets of rotameters with ranges of 0.05-0.5, 2-20, and 20-200 cubic feet per hour (CFH) are used to measure the air volume flow rate, while a rotameter with a range of 0.8-8 liters per minute (LPM) is employed to measure the water volume flow rate. Experiments are conducted at J_G values between 0.079 and 2.8 m/s and J_L between 0.079 and 0.32 m/s. The accuracy of the water rotameter and air rotameter is ±4% of full scale. The inlet and outlet of the hot and cold streams of the test section are equipped with T-type thermocouples that have an accuracy of ±0.4%. With an accuracy of ± 0.065% of ΔP span, the Yokogawa EJA110A accurately measures the pressure difference between the inlet and outlet ports of the cold stream. The uncertainties in the measured parameters are calculated using the root sum of square method. The average uncertainties in superficial gas velocity, superficial liquid velocity, and pressure drop are ±0.00794 m/s, ±0.0344 m/s, and ±3.7%, respectively. The test section, which is a PHE, is intended to function in both counter-flow and single-pass modes. A hot stream flows vertically downward, while a cold stream flows vertically upward. The test section is composed of two copper plates, an acrylic plate, and an aluminum plate to observe the two-phase flow pattern, as illustrated in Fig. 2. The two-phase flow pattern of the cold stream is captured using a high-quality digital camera and a digital camcorder. To examine the ΔP of two-phase flow, the acrylic and aluminum plates are replaced by a copper plate, and the PHE is insulated to prevent heat loss. Copper foam with a pore density of 40 PPI, a porosity of 0.932, permeability of 6.62 x 10^{-8} m^2, and an effective thermal conductivity of 10.1 W/m K is placed in the passage of the cold stream. Grooved copper foam (GCF) and rectangular copper foam (CF) are two forms inserted into the PHE. A wire-cutting machine is used to form the rectangular copper foam, which has dimensions of 25.2 cm x 8.4 cm x 0.5 cm (length x width x thickness) (Fig. 3a). A groove with a checkered pattern and a rectangular depth of 0.3 centimeters is carved into the rectangular copper foam to create the grooved copper foam. The square pin copper foam has a center-to-center distance of 10 mm in both the horizontal and vertical planes (Fig. 3b). This experiment employs two copper foams with groove widths (w) of 4 and 6 mm.

3. Data reduction

3.1 Superficial gas and liquid velocity

The air-water flow pattern within the PHE is determined by the superficial liquid velocities (J_L) and superficial gas velocities (J_G). These velocities are determined using the following equations:

$$J_L = \dot{V}_L / A \quad (1)$$

$$J_G = \dot{V}_G / A \quad (2)$$

$$A = wb \quad (3)$$

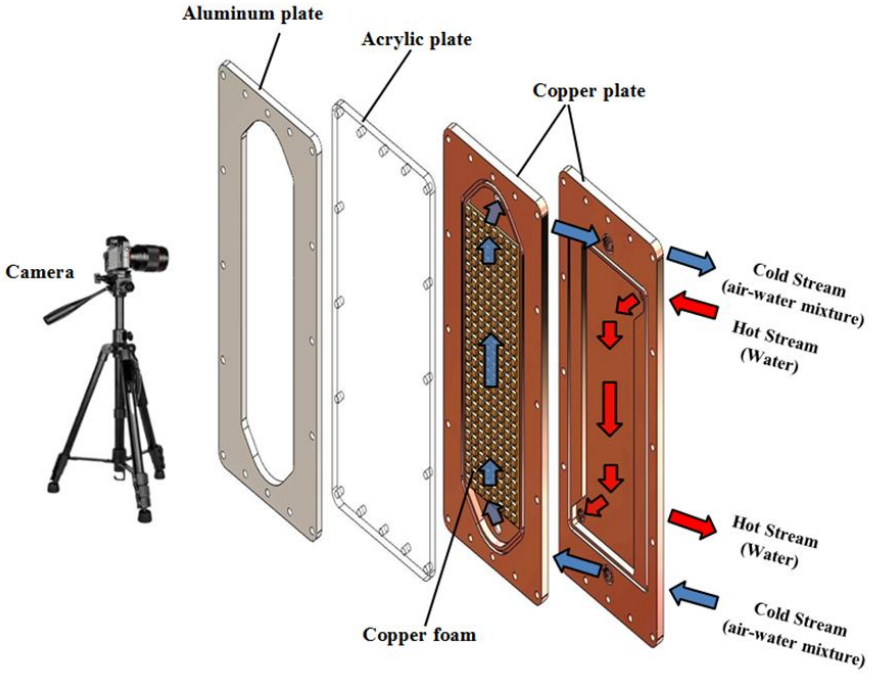

Fig. 2: Schematic of the test section for observing flow patterns.

where A is the flow area of the passage, w is the plate width, and b is the distance between plates. $\dot{V}_L$ and $\dot{V}_G$ are volume flow rates of liquid and volume flow rates of gas, respectively.

3.2 Frictional pressure drop

3.2.1 Single-phase pressure drop

The following equation expresses the relationship between the total pressure drop (ΔP_T) and the frictional pressure drop (ΔP_F), gravitational pressure drop (ΔP_G), and pressure loss at the inlet and outlet port (ΔP_M) inside the PHE.

$$\Delta P_F = \Delta P_T - \Delta P_G - \Delta P_M \quad (4)$$

A differential pressure transmitter is employed to measure the total pressure drop. The gravitational pressure drop is determined as follows:

$$\Delta P_G = gL/\upsilon \quad (5)$$

The following correlation is employed to determine the pressure loss at the inlet and outlet ports.[13]

$$\Delta P_M \cong 1.5\left(\frac{G^2\upsilon}{2}\right) \quad (6)$$

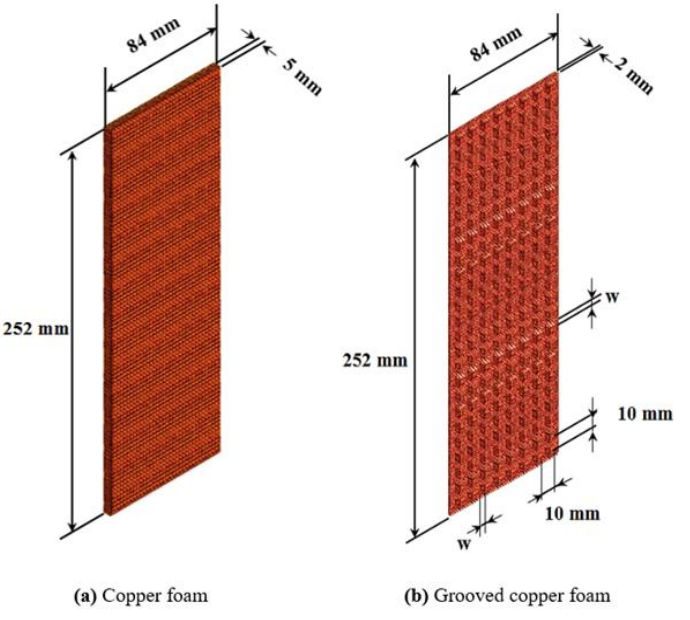

(a) Copper foam **(b)** Grooved copper foam

Fig. 3: Two types of copper foam.

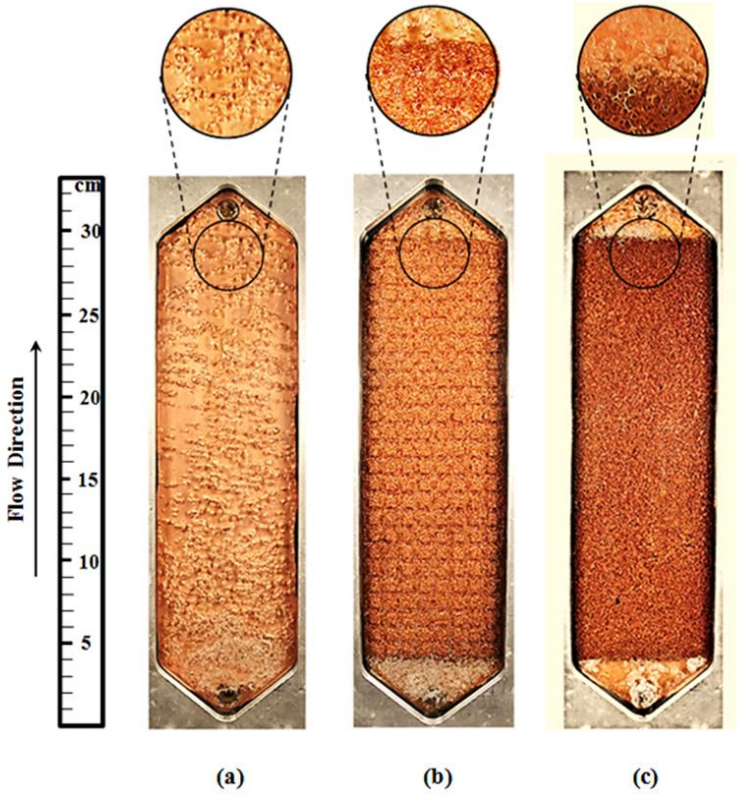

Fig. 4: Bubbly flow at J_L = 0.278 m/s and J_G = 0.0794 m/s. (a) PHE, (b) PHE_GCF, and (c) PHE_CF.

The Fanning friction factor for single-phase flow can be calculated as:

$$f = \frac{dP_F D_h}{2G^2 \upsilon L} \quad (7)$$

The Reynolds number for single-phase flow is determined from:

$$Re = \frac{\rho V D_h}{\mu} \quad (8)$$

and $$D_h = \frac{4A}{P} \quad (9)$$

where ρ *is* density, V is velocity, μ *is* viscosity, D_h is hydraulic diameter, L is the vertical distance between inlet and outlet ports, and P is the perimeter of the flow passage.

Calculation of the ΔP_F in a PHE can be done using Eq. (4) to (6). An equation to determine the specific volume is:

$$\upsilon_m = \upsilon_f + x\upsilon_{fg} \quad (10)$$

Additionally, for a two-phase flow, the acceleration pressure drop is incorporated into the total pressure drop. This is determined based on a homogeneous model, as shown in the following equation:

$$\Delta P_G = G^2 \upsilon_{fg} \Delta x \quad (11)$$

where g is gravitational acceleration, υ is the specific volume, υ_f is the specific volume of liquid, υ_{fg} is the difference in specific volume between vapor and liquid phases, x is the quality, Δx is the difference in quality between the inlet and

3.2.2 Two-phase pressure drop

Table 1: Single-phase pressure drop correlation through porous media.

Authors	Correlation
Nilpueng *et al.*[14]	$\frac{\Delta P}{L} = 110\frac{\mu}{\varepsilon D_h^2}V + 1.45\frac{\rho}{\varepsilon^2 D_h}V^2, \quad D_h = \frac{1.394\varepsilon(d_f + d_p)}{(1-\varepsilon)^{0.25}}$
Dietrich *et al.*[19]	$\frac{\Delta P}{L} = 4\frac{f\rho V^2}{2D_h}, \quad \mathrm{f} = 0.112\, Re^{-0.1508}\, D\, a^{-0.5338}$
Bhattacharya *et al.*[20]	$\frac{\Delta P}{L} = \frac{\mu}{K}V + \frac{\rho f}{\sqrt{K}}V^2, f = 0.0095G^{-0.8}\sqrt{\frac{\varepsilon}{3(\chi-1)}}\left(1.18\sqrt{\frac{(1-\varepsilon)}{3\pi}}\frac{1}{G}\right)^{-1}, G = 1 - e^{-\frac{1-\varepsilon}{0.04}}$
Beavers and Sparrow[21]	$\frac{\Delta P}{L} = 2f_K\left(\frac{1}{D_H}\rho\frac{V^2}{2}\right), f_K = \frac{1}{\mathrm{Re_K}} + 0.074, \mathrm{Re_K} = \frac{\rho V D_K}{\mu}, D_K = \sqrt{K}$

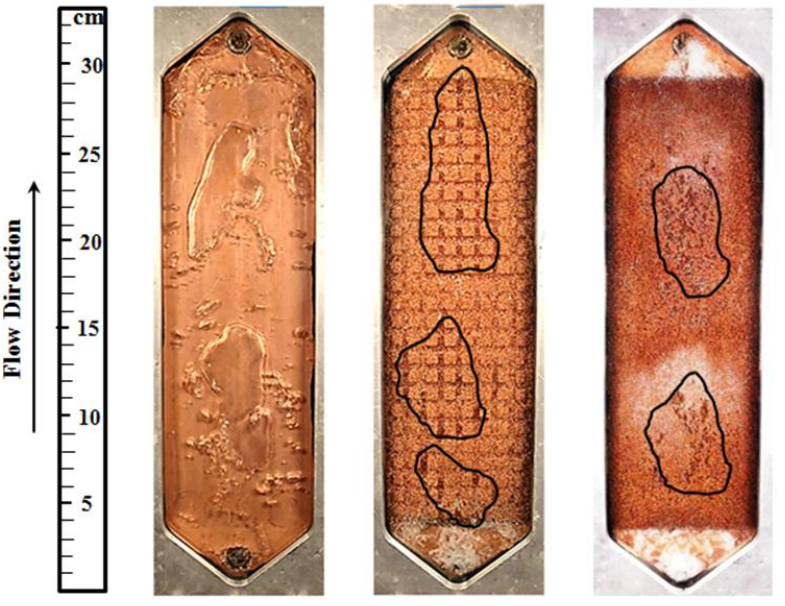

Fig. 5: Churn flow at J_L = 0.198 m/s and J_G = 0.397 m/s. (a) PHE, (b) PHE_GCF, and (c) PHE_CF.

between the inlet and outlet, and G is mass flux.

3.3 Two-phase multiplier

Correlations for the two-phase multiplier (ϕ_L^2) are derived from experimental frictional pressure drop data and normally applied in practical scenarios. This multiplier represents the ratio of the pressure gradient in two-phase flow $(dP_F/dz)_{TP}$ to that in the liquid phase $(dP_F/dz)_L$, as given by the following equation:

$$\phi_L^2 = \frac{(dP_F/dz)_{TP}}{(dP_F/dz)_L} \tag{12}$$

A traditional and widely accepted two-phase multiplier correlation, proposed by Lockhart and Martinelli,[16] is based on the C parameter and the Martinelli parameter (X), as expressed below.

$$\phi_L^2 = 1 + \frac{C}{X} + \frac{1}{X^2} \tag{13}$$

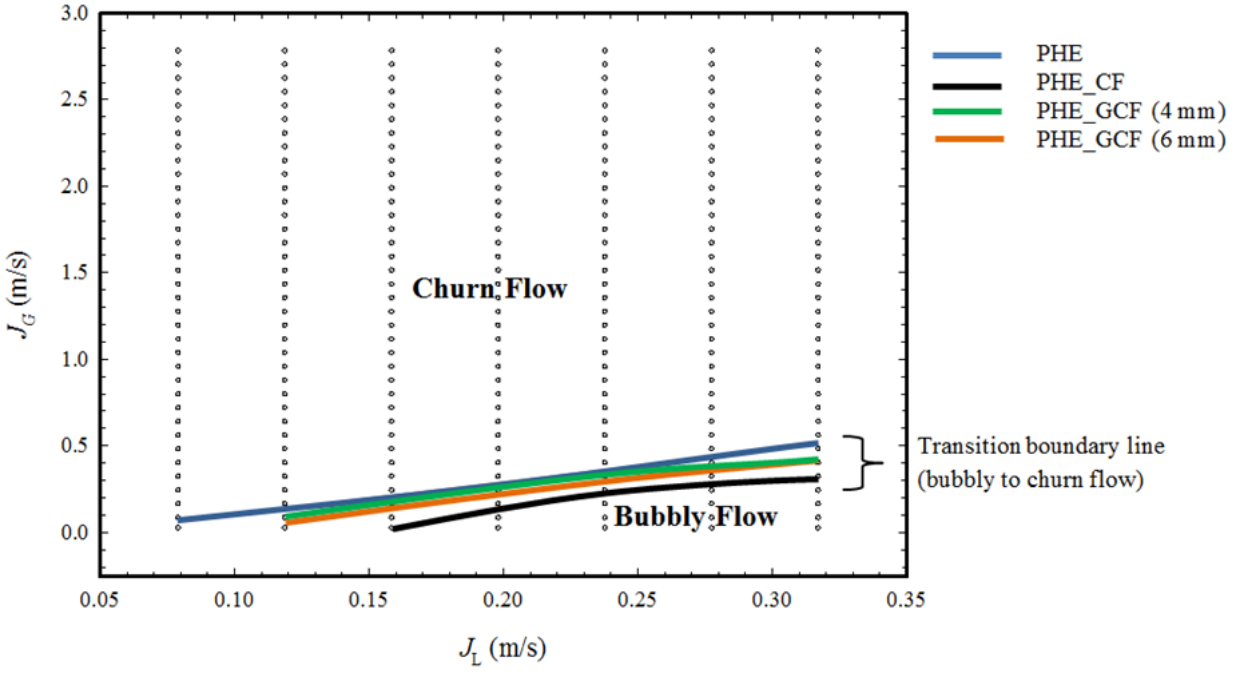

Fig. 6: Flow pattern map of air-water two-phase flow in the PHE, PHE_GCF and PHE_CF.

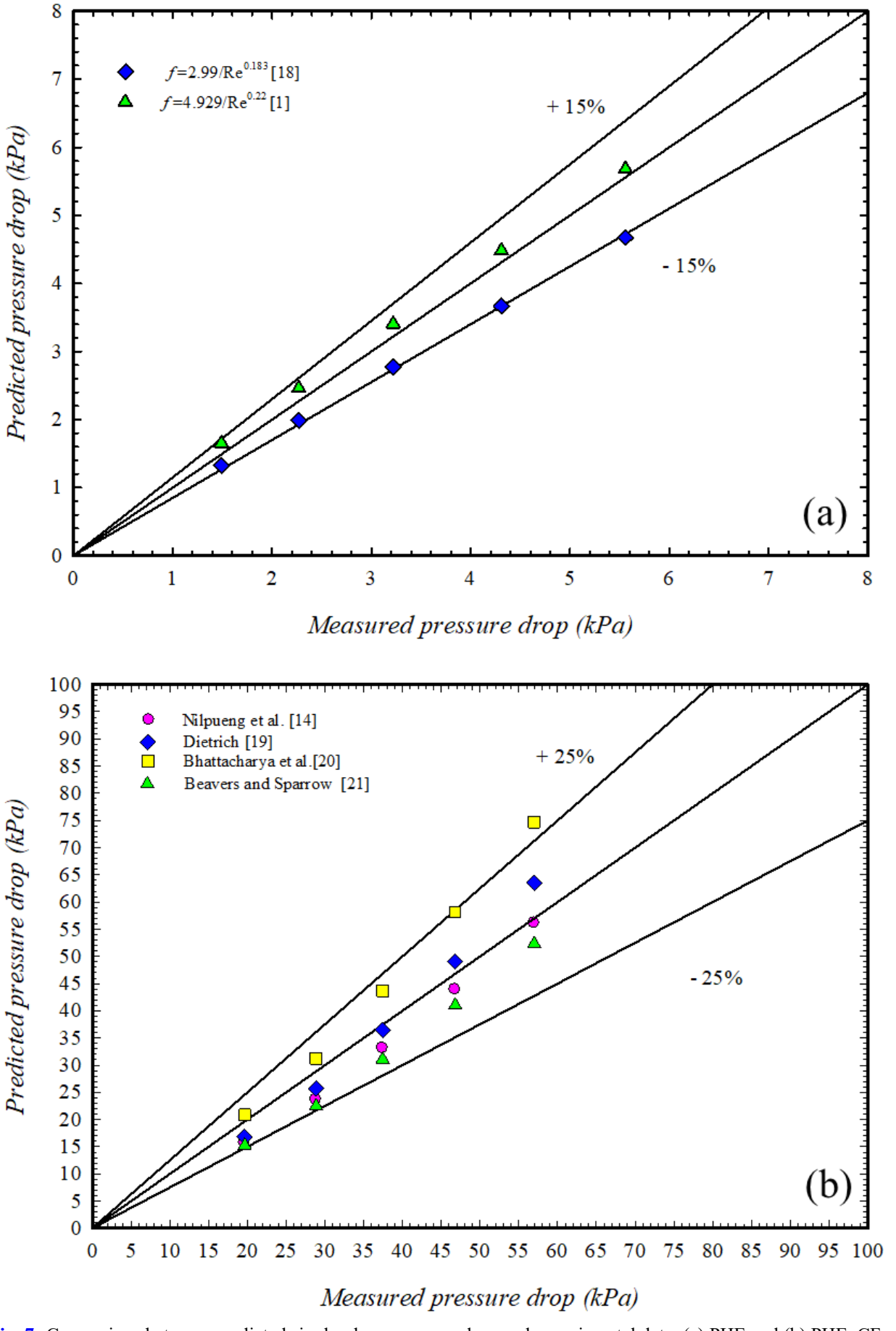

Fig. 7: Comparison between predicted single-phase pressure drop and experimental data. (a) PHE and (b) PHE_CF.

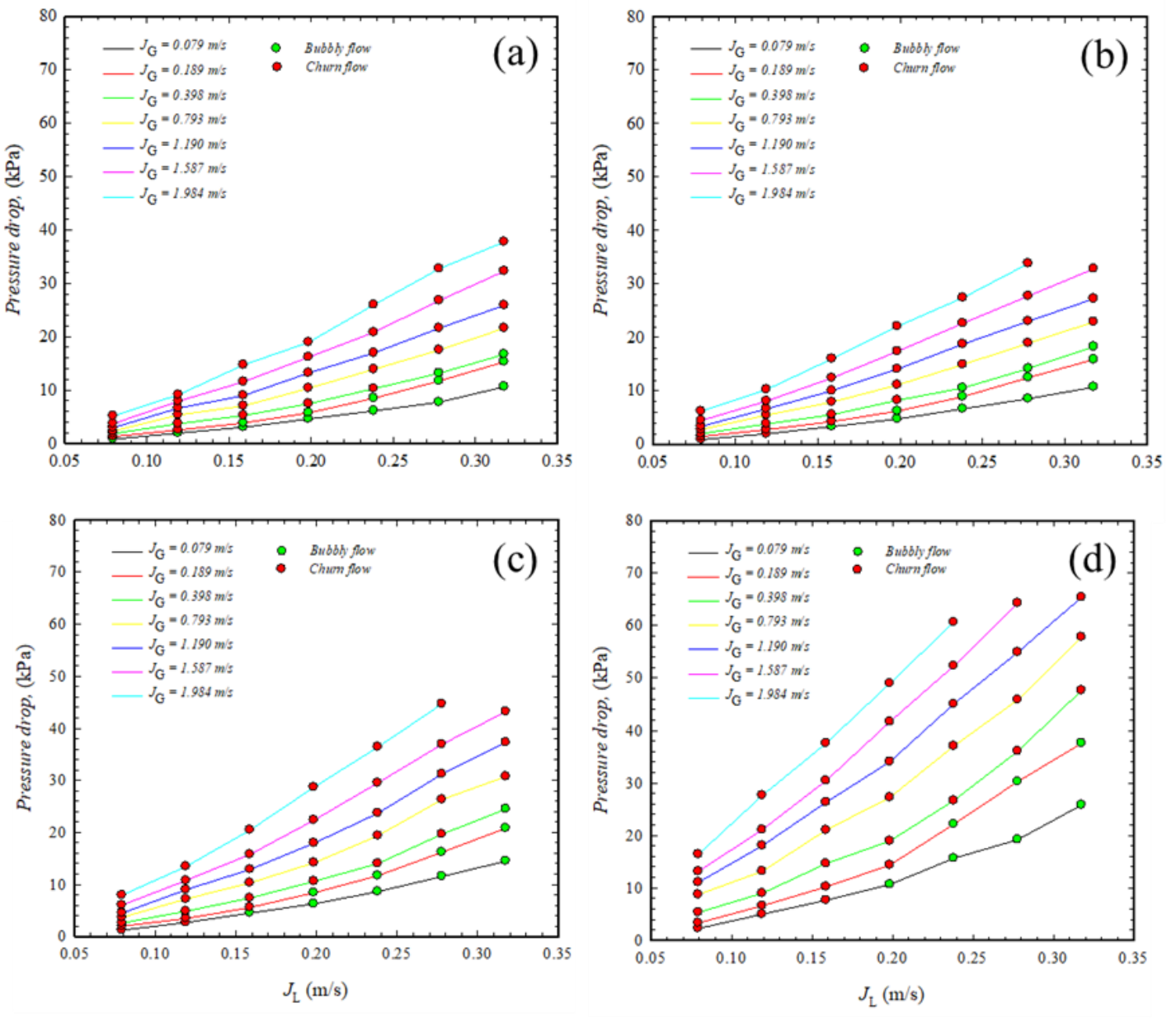

Fig. 8: Effect of superficial liquid velocity, superficial gas velocity and flow pattern on pressure drop. (a) PHE, (b) PHE_GCF (6 mm), (c) PHE_GCF (4 mm), and (d) PHE_CF.

According to Chisholm,[17] the C parameter is a constant that represents the flow conditions of both liquid and gas. It typically ranges from 5 to 20. For *e.g*, *C* is 5 when each phase is in laminar flow and 20 when each phase is in turbulent flow. *X* is a quantitative measure that compares the pressure gradient in the liquid phase $(dP_F/dz)_L$ to the pressure gradient in the gas phase $(dP_F/dz)_G$. It is calculated using the following formulae:

$$X^2 = \frac{(dP_F/dz)_L}{(dP_F/dz)_G} \quad (14)$$

$$(dP_F/dz)_L = \frac{2f_L G_L^2}{\rho_L D_h} \quad (15)$$

$$(dP_F/dz)_G = \frac{2f_G G_G^2}{\rho_G D_h} \quad (16)$$

4. Results and discussion

The flow patterns and ΔP of two-phase air-water flow in the PHEs are presented in this section.

4.1 Two-phase flow patterns

Observations are conducted by utilizing still images captured using a high-quality digital camera and a digital camcorder to characterize the two-phase water-air flow patterns within the PHEs. For the PHE_GCF and PHE_CF, clear portions of the images correspond to the gas phase, while the blurred portions represent the liquid phase. Within a PHE, the two-phase flow patterns of air and water can be classified into two primary patterns.

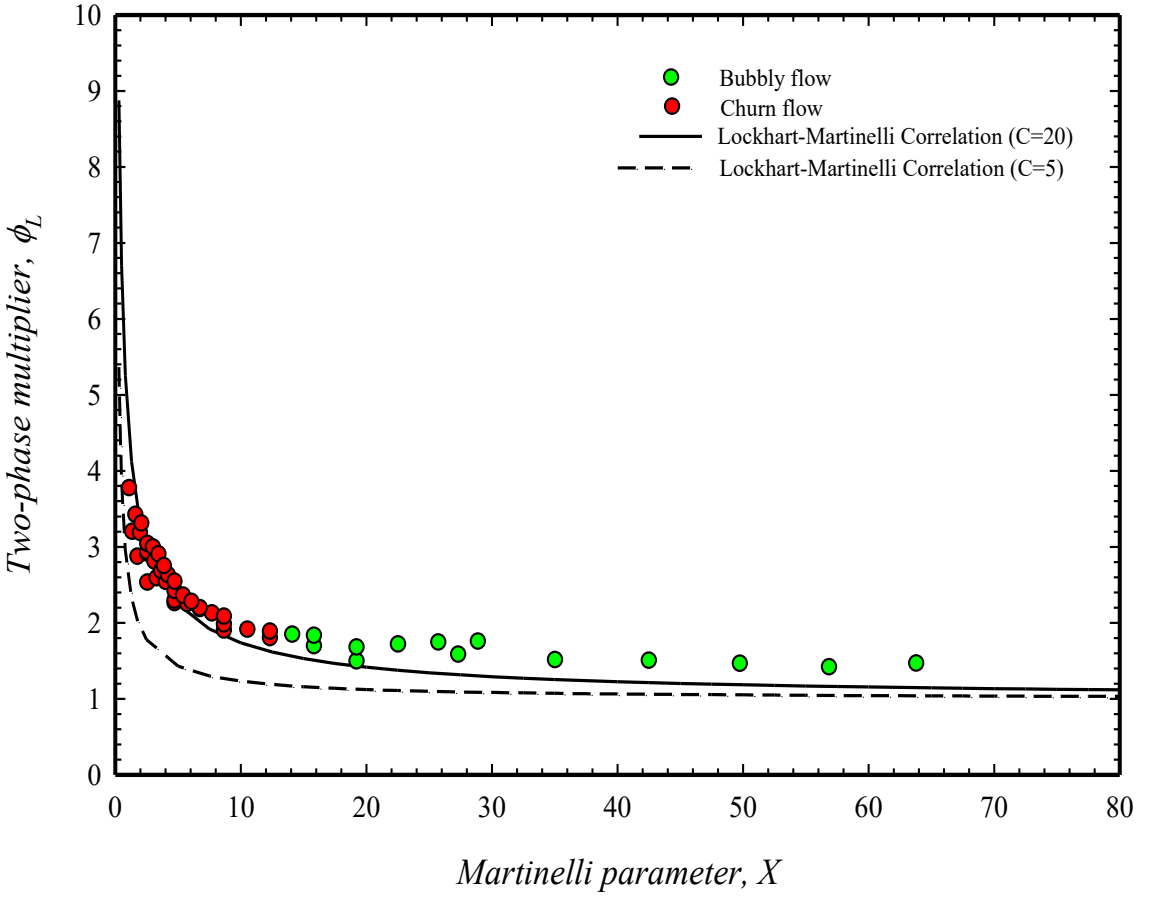

Fig. 9: Relationship between the Martinelli parameter and two-phase multiplier in a PHE.

- *Bubbly flow*

In the bubbly flow pattern, the gas phase is dispersed within the liquid phase, forming a continuous phase that flows through the passage. The bubbles (gas phase) vary in size (Fig. 4a), with larger bubbles resulting from the coalescence of smaller ones. The size of the bubbles in the passage tends to increase at higher J_G values while maintaining a constant J_L. Bubble flow is observed within the copper foam structure of the PHE_CF (Fig. 4c), whereas in the PHE_GCF, bubbles primarily flow along the vertical grooves (Fig. 4b). Furthermore, under similar J_G and J_L values, larger bubble sizes are observed when the size of the groove is wider.

- *Churn flow*

As the J_G value increases at a given J_L, small dispersed gas bubbles within the continuous liquid flow coalesce into larger, elongated bubbles. These elongated bubbles ascend rapidly, generating strong interfacial shear that induces partial downward liquid motion near the wall. This countercurrent liquid motion promotes bubble deformation and breakup (see Fig. 5a). As a result, the flow transitions directly into the churn flow regime without the formation of stable slug structures. The churn regime is characterized by chaotic and oscillatory liquid movement in both the upward and downward directions. This flow phenomenon resembles that seen in a PHE_GCF (Fig. 5b). However, the elongated bubbles in the PHE_GCF are generally longer compared to those in a PHE. In a PHE_CF, bubble breakup induced by the downward liquid flow promotes air–liquid mixing, resulting in the formation of a mist-like cluster (Fig. 5c).

Using observations of the flow patterns, a flow pattern map is identified as a function of J_G and J_L for PHE, PHE_GCF, and PHE_CF, as shown in Fig. 6. At a certain J_L, a rise in J_G transforms the flow from bubbly flow to churn flow. When comparing bubbly flow patterns among PHE, PHE_GCF, and PHE_CF, the bubbly flow region in the channel is smaller than that observed in the PHE due to the presence of copper

Table 2: Proposed friction factor correlations for single-phase flow in the test section.

Test section	Correlation	
PHE	$f = 1.83 / Re^{0.102}$,	1875< Re <3750
PHE_GCF (4 mm)	$f = 7.30 / Re^{0.256}$,	1875< Re <3750
PHE_GCF (6 mm)	$f = 2.18 / Re^{0.117}$,	1875< Re <3750
PHE_CF	$f = 17.67 / Re^{0.288}$,	1875< Re <3750

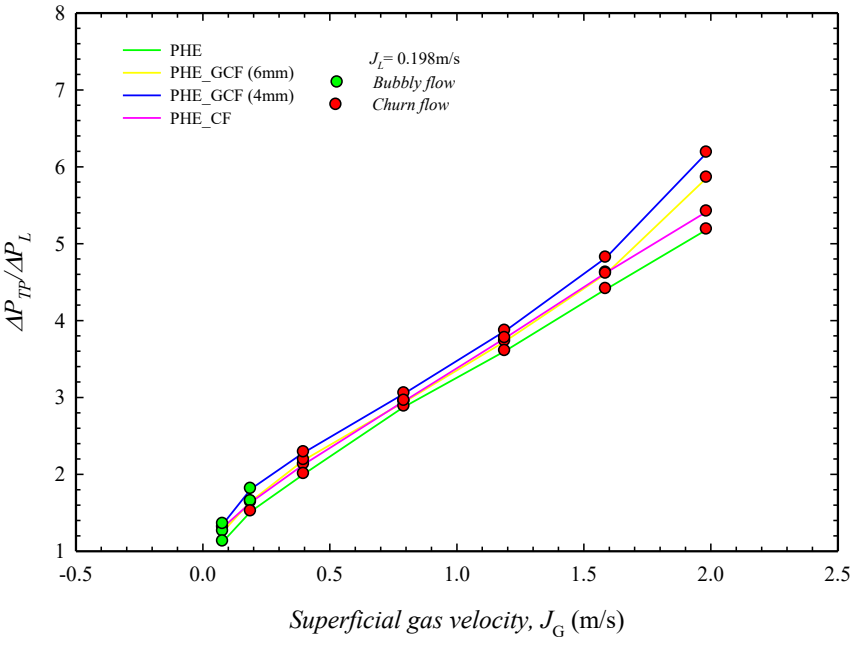

Fig. 10: Effect of flow pattern on the pressure drop ratio.

foam. The bubbly flow region is larger when the copper foam is grooved. However, the churn flow region in the PHE is smaller compared to the PHE_GCF and PHE_CF with the largest churn flow region occurring in the PHE_CF. This may occur because the copper foam structure in the passage promotes formation of elongated bubbles and reduces their breakdown. Consequently, the bubbly flow region in a PHE_CF is the largest, while the churn flow region is the narrowest.

4.2 Pressure drop

4.2.1 Single-phase flow

Before analyzing the ΔP_{TP}, the ΔP_{SP} for the PHE and PHE_CF is validated against existing correlations. As shown in Fig. 7a, the ΔP_{SP} for the PHE, calculated using the friction factor correlations by Nilpueng and Wongwises.[1] and Kakac and Liu[18] is consistent with the current experimental data. The mean absolute deviations (MADs) of the correlations are 7.59%and 12.9%, respectively. Similarly, when comparing the correlations for ΔP_{SP} through porous media against the present data for the PHE_CF (Fig. 7b), the deviations are within ±25%, especially for the correlations proposed by Dietrich[19] and Nilpueng *et al.*,[14] which had MADs of 8.85% and 11.55%, respectively. The details of the ΔP_{SP} correlations through porous media are depicted in Table. 1.

A new correlation for the single-phase friction factor in a PHE has been developed and is utilized to calculate the two-phase multiplier, as illustrated in Table 2. This correlation is derived from the current experimental data. Moreover, according to the literature review, several methods exist for predicting single-phase flow behaviors through porous structures, with a common approach being the use of friction factor correlations. Therefore, a correlation for the Fanning friction factor inside the PHE_GCFs and PHE_CFs is proposed. The proposed correlations for the friction factor achieved MADs of 0.24%, 0.41%, 0.64%, and 0.36% compared to the measured data for the PHE, PHE_GCF (6 mm and 4 mm), and PHE_CF, respectively.

4.2.2 Two -phase flow

Table 3: Earlier correlations for ϕ_L^2 in two-phase flow through the passage.

Authors	Correlation
Lockhart-Martinelli[16,17]	$\phi_L^2 = 1 + \frac{C}{X} + \frac{1}{X^2}, X^2 = \frac{(dP_F/dz)_L}{(dP_F/dz)_G}, C = 20$
Friedel correlation[22]	$\phi_L^2 = E + \frac{3.24FH}{Fr_H^2 We_L^{0.035}}, Fr_H = \frac{G^2}{gd\rho_H^2}, E = (1-x^2) + x^2\frac{\rho_L f_G}{\rho_G f_L},$ $F = x^{0.78}(1-x)^{0.224}, H = \left(\frac{\rho_L}{\rho_G}\right)^{0.91}\left(\frac{\mu_G}{\mu_L}\right)^{0.19}\left(1-\frac{\mu_G}{\mu_L}\right)^{0.7}, We_{\frac{GD_h}{\sigma\rho_H}L}$
Zhang *et al.*[23]	$\phi_L^2 = 1 + \frac{C}{X} + \frac{1}{X^2}, C = 21[1 - exp(-0.358/Lo^*)], Lo^* = \left[\frac{\sigma}{g(\rho_f - \rho_g)}\right]^{0.5}\frac{1}{D_h}$

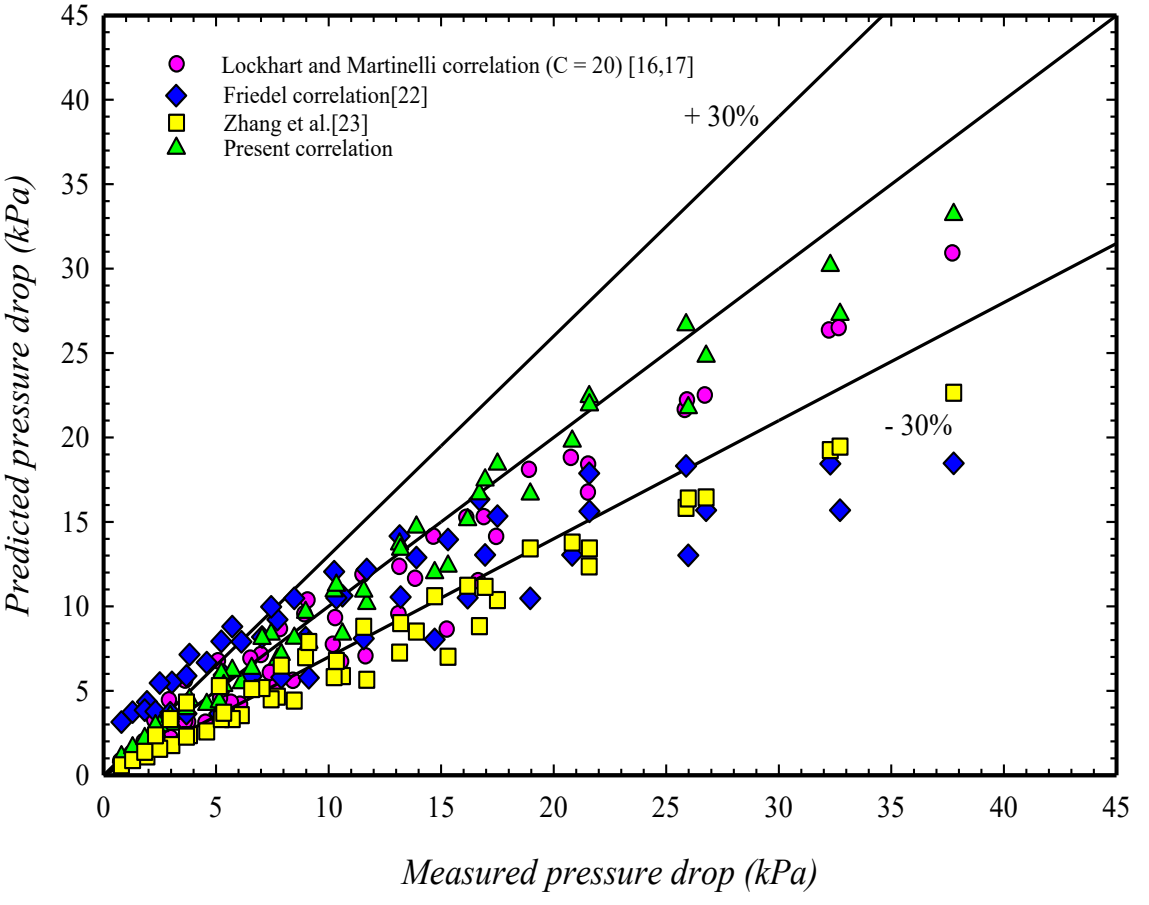

Fig. 11: Comparison between measured and predicted two-phase pressure drop in a PHE.

Considering the ΔP of two-phase air-water flow through the PHE, PHE_CF, and PHE_GCF from Fig. 8, the data clearly show that the ΔP_{TP} increases significantly with the J_G and J_L values. Inserting copper foam within the PHE results in a notable increase in ΔP_{TP}. Specifically, the ΔP_{TP} in the PHE_CF shows an approximate 2.63 times increase compared to the PHE. This increase can be attributed to friction between the wall of the passage and the air-water mixture, as well as friction between the gas and liquid phases, which becomes stronger at higher J_G and J_L values. Furthermore, the contact surface area and tortuous structure of the copper foam contribute to increased friction and flow resistance, resulting in a much higher ΔP_{TP} in the PHE_CF compared to the PHE.

For the PHE_GCF, the ΔP_{TP} is reduced relative to the PHE_CF and decreases with increased groove width. In comparison with the PHE_CF, the ΔP_{TP} of the PHE_GCF is decreased by approximately 48.0% and 59.3% for groove widths of 4 mm and 6 mm, respectively. This reduction occurs since the air-water mixture primarily flows within the grooves of the copper foam in the PHE_GCF. This flow behavior reduces flow resistance due to the decreased contact surface area and less tortuous path, especially with a wider groove. Therefore, the ΔP in the PHE_GCF is lower than in the PHE_CF and decreases further with a wider groove.

Table 4: Two-phase flow correlations of ϕ_L^2 in passage filled with metal foam.

$$\phi_L^2 = 1 + \frac{C}{X} + \frac{1}{X^2}, X = \left(\frac{\mu_L}{\mu_G}\right)^{0.5}\left(\frac{1-x}{x}\right)^{0.5}\left(\frac{\upsilon_L}{\upsilon_G}\right)^{0.5}$$

Authors	Correlation
Ji and Xu[24]	$C = 0.025G^{1.801}e^{8.021x}d_m^{0.455}$
Hu *et al.*[25]	$C = 27.27G^{-0.38}e^{-0.477x}d_p^{-0.181}$
Tourvieille *et al.*[26]	$C = 121.41G^{0.54}e^{9.90x}d_{cell}^{0.68}$
Ku *et al.*[27]	$C = 120.57G^{0.2}d_m^{0.15}x^{0.458}$

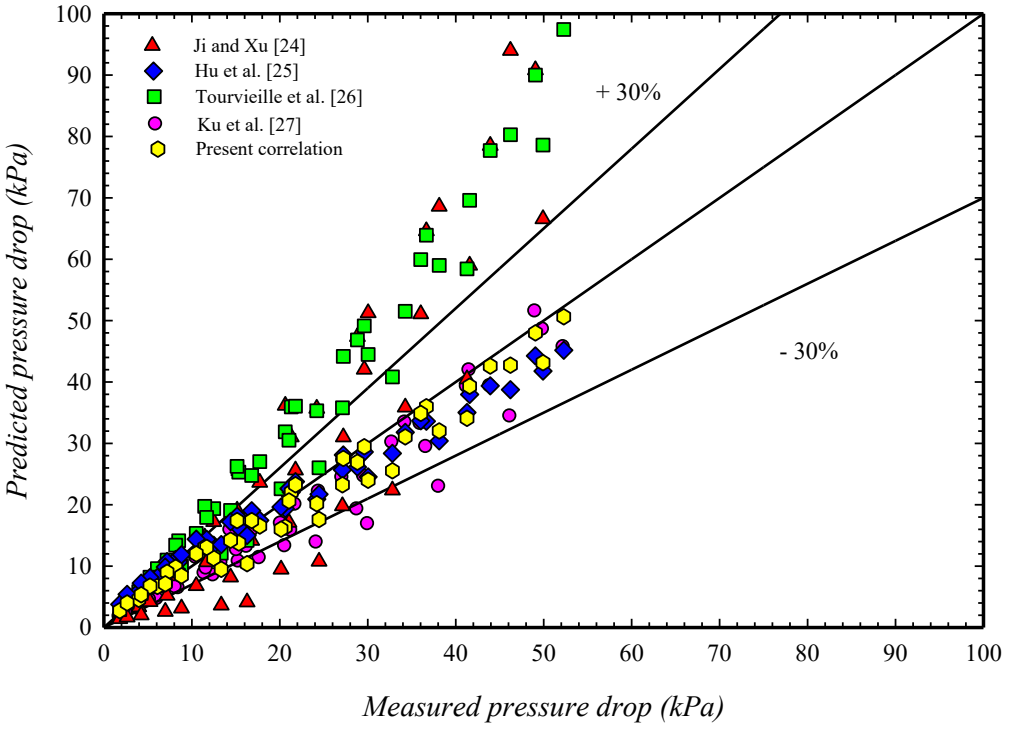

Fig. 12: Comparison between measured and predicted two-phase pressure drop in a PHE_CF.

Based on the measured frictional pressure drops within a PHE, the two-phase multipliers are determined and plotted against the Martinelli parameters, as illustrated in Fig. 9. Analysis reveals that the trend of these multipliers aligns with the predictions of the Lockhart–Martinelli correlation, showing MAD values of 36.7% and 10.3% for C parameters of 5 and 20, respectively. These results suggest that the two-phase flow in this PHE (narrow rectangular channel) corresponds to turbulent conditions for both the liquid and gas phases, with a C-parameter value of approximately 20.

The impact of flow pattern on the ΔP ratio (the ratio of the pressure drop in the two-phase flow to the pressure drop in the liquid phase, $\Delta P_{TP}/\Delta P_L$) under the specified conditions (J_L =0.198 m/s and J_G =0.079 - 0.198 m/s), as shown in Fig. 10, is examined. Transition from bubbly flow to churn flow increases the pressure drop ratio in each type of PHE. The average pressure drop ratio increases by a factor of 2.2 during the transition from bubbly to churn flow. When the flow changes from bubbly flow to churn flow, the oscillatory movement caused by the breakdown of elongated bubbles further intensifies turbulence in the air-water mixture. This causes an elevated ΔP ratio in churn flow compared to bubbly flow.

4.2.3 Development of a correlation for two-phase pressure drop

Before generating the ΔP_{TP} correlation, existing correlations for frictional ΔP during air-water two-phase flow in passages and passages with metal foam are evaluated against experimental data obtained from the PHE and PHE_CF. The previous correlations for frictional ΔP in gas-liquid two-phase flows in passages and passages with metal foam inserts are based on Eq. 12 and 13. Details of ϕ_L^2 are presented in Tables. 3 and 4.

As shown in Fig. 11, ΔP_{TP} calculated using existing correlations is in good agreement with the measured results, especially the Lockhart and Martinelli[16,17] correlation, which gives a mean absolute deviation (MAD) of 19.7%. Conversely, some correlations exhibit higher deviations, with MADs of 44.1% and 34.0% for the Friedel[22] and Zhang *et al.*[23] correlations, respectively. For the PHE_CF, comparisons of the present ΔP_{TP} align well with the correlations from Ku *et al.*[27] and Hu *et al.*,[25] yielding mean absolute deviations (MADs) of 16.5% and 21.8%, respectively (Fig. 12). However, some previous correlations overestimate the experimental results by 30%, with MAD values of 51.2% and 43.7% for the calculated results from Tourvieille *et al.*[26] and Ji and Xu,[24] respectively.

Comparison of results for ΔP_{TP} in the PHE and PHE_CF shows high deviations from certain correlations, possibly due to differences in testing conditions and flow passage configurations. The current study presents a novel correlation for forecasting the change in ΔP_{TP}. This correlation is defined in terms of a two-phase multiplier, as demonstrated by the following equations.

For PHE

$$\phi_L^2 = \frac{13.035}{X^{0.497}} \quad (17)$$

For PHE_GCF and PHE_CF

$$\phi_L^2 = \frac{11.542}{X^{0.487}\Phi^{0.256}} \quad (18)$$

A two-phase multiplier is formulated based on the Martinelli parameter (X) and the copper foam filling ratio (Φ). The filling ratio of the copper foam is the proportion of the volume occupied by the copper foam within the rectangular passage. This concept is applied to the PHE_GCF (6 mm and 4 mm) and PHE_CF, which have filling ratios of 0.49, 0.6, and 1, respectively. The proposed correlations exhibit good agreement with the measured data, with MADs of 10.48% for the PHE, and 10.85% for both the PHE_GCF and PHE_CF.

5. Conclusion

This paper studies the air-water two-phase flow pattern and ΔP in a PHE, PHE_GCF, and PHE_CF. Copper foam with a checkered pattern groove and varying groove widths, a porosity of 0.932, and a pore density of 40 PPI is used. Experiments are conducted at J_L values between 0.079 and 0.32 m/s and J_G between 0.079 and 2.8 m/s. The experimental results can be summarized as follows.

1) The two-phase flow patterns in the PHE, PHE_GCF, and PHE_CF are categorized into two types, churn flow, and bubbly flow. Bubbly flow regions in the PHE_GCF and PHE_CF decrease when compared to those in the PHE. Churn flow regions are smallest in the PHE and largest in the PHE_CF.

2) The ΔP_{TP} within the PHE, PHE_CF, and PHE_GCF increased significantly with higher J_G and J_L values. The PHE_CF exhibited a substantial increase in ΔP_{TP} compared to the PHE, while the ΔP_{TP} in the PHE_GCF was lower than in the PHE_CF and decreased as groove widths widened.

3) The average ΔP ratio increased by 2.2 times during the transition from bubbly to churn flow under the specified conditions and across all types of PHEs.

4) Existing correlations for ΔP_{TP} showed high deviations from experimental data from the PHE and PHE_CF. The proposed ΔP_{TP} correlations, incorporating the Martinelli parameter and the copper foam filling ratio, demonstrated MADs of 10.48% for the PHE and 10.85% for both the PHE_GCF and PHE_CF.

Acknowledgments

The first author thanks the financial support provided by the National Research Council of Thailand (NRCT) under Grant No. N41A640148. The second author acknowledges The Thailand Science Research and Innovation (TSRI), and National Science, Research and Innovation Fund (NSRF) Fiscal year 2025 under Grant No. FRB680074/0164. The authors sincerely appreciate and thank Mr. Tanachon Chomamuang for his valuable help during the experiments.

Conflict of Interest

The authors declare no conflict of interest.

Supporting Information

Not applicable.

Nomenclature

A	: flow area, m^2
D_h	: hydraulic diameter, m
dP/dz	: pressure gradient, Pa/m
f	: friction factor
g	: gravitational acceleration, m/s^2
G	: mass flux, kg/m^2 s
J_G	: superficial gas velocity, m/s
J_L	: superficial liquid velocity, m/s
L	: vertical distance between ports, m
PHE	: plate heat exchanger
PHE_CF	: plate heat exchanger with copper foam
PHE_GCF	: plate heat exchanger with grooved copper foam
V	: velocity, m/s
$\dot{V}$	: volume flow rate, m^3/s
X	: Martinelli parameter
ΔP	: pressure drop, Pa
Greek symbols	
u	: specific volume, $m^3/$ kg
ϕ_L^2	: two-phase multiplier
μ	: dynamic viscosity, kg/ m s
Φ	: copper foam filling ratio

CRediT Statement

Kitti Nilpueng: Data curation, Formal analysis, Investigation, Writing-original draft, Writing-reviewing and editing.

Somchai Wongwises: Conceptualization, Supervision, Funding acquisition, Investigation, Writing-reviewing and editing.

References

[1] K. Nilpueng, S. Wongwises, Two-phase gas–liquid flow characteristics inside a plate heat exchanger, *Experimental Thermal and Fluid Science*, 2010, **34**, 1217–1229, doi: 10.1016/j.expthermflusci.2010.05.001.

[2] V. Grabenstein, A.-E. Polzin, S. Kabelac, Experimental investigation of the flow pattern, pressure drop, and void fraction of two-phase flow in the corrugated gap of a plate heat exchanger, *International Journal of Multiphase Flow*, 2017, **91**, 155–169, doi: 10.1016/j.ijmultiphaseflow.2017.01.012.

[3] L. Wei, L.-M. Pan, Y.-M. Zhao, Q.-Y. Ren, W.-Z. Zhang, Numerical study of adiabatic two-phase flow patterns in vertical rectangular narrow channels, *Applied Thermal Engineering*, 2017, **110**, 1101–1110, doi: 10.1016/j.applthermaleng.2016.09.007.

[4] C. Jiang, B. Bai, Flow patterns and pressure drop of downward two-phase flow in a capsule type plate heat

exchanger, *Experimental Thermal and Fluid Science*, 2019, **103**, 347–354, doi: 10.1016/j.expthermflusci.2019.01.026.
[5] D. Lee, D. Kim, S. Yun, Y. Kim, Two-phase flow patterns and pressure drop of a low GWP refrigerant R-1234ze(E) in a plate heat exchanger under adiabatic conditions, *International Journal of Heat and Mass Transfer*, 2019, **145**, doi: 10.1016/j.ijheatmasstransfer.2019.118816.
[6] S. Buscher, Digital image analysis of gas-liquid flow in a cross-corrugated plate heat exchanger channel: A feature-based approach on various two-phase flow patterns, *International Journal of Multiphase Flow*, 2022, **154**, doi: 10.1016/j.ijmultiphaseflow.2022.104149.
[7] M. Vatani, D. D. Ganji, Experimental study of two-phase flow patterns through an inclined rectangular channel with horizontal and vertically upward directions, *Alexandria Engineering Journal*, 2023, **62**, 445–453, doi: 10.1016/j.aej.2022.07.043.
[8] S. Passoni, A. Ferrario, M. E. Ricotti, R. Mereu, Experimental investigation of two-phase flow in Chevron-type compact plate heat exchangers: A study on pressure drops and flow regimes visualization, *Applied Thermal Engineering*, 2024, **242**, doi: 10.1016/j.applthermaleng.2024.122542.
[9] Y. Zhu, H. Hu, S. Sun, G. Ding, Flow boiling of refrigerant in horizontal metal-foam filled tubes: Part 1 – Two-phase flow pattern visualization, *International Journal of Heat and Mass Transfer*, 2015, **91**, 446–453, doi: 10.1016/j.ijheatmasstransfer.2015.07.096.
[10] G. B. Abadi, C. Moon, K. C. Kim, Experimental study on single-phase heat transfer and pressure drop of refrigerants in a plate heat exchanger with metal-foam-filled channels, *Applied Thermal Engineering*, 2016, **102**, 423–431, doi: 10.1016/j.applthermaleng.2016.03.099.
[11] G. B. Abadi, C. Moon, K. C. Kim, Flow boiling visualization and heat transfer in metal-foam-filled mini tubes – Part I: Flow pattern map and experimental data, *International Journal of Heat and Mass Transfer*, 2016, **98**, 857–867, doi: 10.1016/j.ijheatmasstransfer.2016.03.043.
[12] H. E. Ahmed, O. T. Fadhil, W. A. Salih, Heat transfer and fluid flow characteristics of tubular channel partially filled with grooved metal foams, *International Communications in Heat and Mass Transfer*, 2019, **108**, 104336, doi: 10.1016/j.icheatmasstransfer.2019.104336.
[13] K. Nilpueng, L. G. Asirvatham, A. S. Dalkılıç, O. Mahian, H. S. Ahn, S. Wongwises, Heat transfer and fluid flow characteristics in a plate heat exchanger filled with copper foam, *Heat and Mass Transfer*, 2020, **56**, 3261–3271, doi: 10.1007/s00231-020-02921-x.
[14] K. Nilpueng, T. Chomamuang, M. Mesgarpour, O. Mahian, S. Wongwises, Thermal-hydraulic performance of a plate heat exchanger with grooved copper foam, *Case Studies in Thermal Engineering*, 2023, **51**, 103525, doi: 10.1016/j.csite.2023.103525.
[15] N. Chandora, A. Mani, S. Advaith, Investigation of heat transfer and pressure drop characteristics in metal-foam filled channels in a plate heat exchanger: A comparative experimental study, *Applied Thermal Engineering*, 2024, **241**, doi: 10.1016/j.applthermaleng.2023.122368.
[16] R. W. Lockhart, R. C. Martinelli, Proposed correlation of data for isothermal two-phase two-component flow in pipes, *Chemical Engineering Progress*, 1949, **45**, 39–48.
[17] D. Chisholm, A theoretical basis for the Lockhart–Martinelli correlation for two-phase flow, *International Journal of Multiphase Flow*, 1967, **10**, 1767–1778, doi: 10.1016/0301-9322(67)90020-3.
[18] S. Kakac, S. Liu, *Heat Exchangers: Selection, Rating and Thermal Design*, Chapter 10, CRC Press, USA, 2002.
[19] B. Dietrich, Pressure drop correlation for ceramic and metal sponges, *Chemical Engineering Science*, 2012, **74**, 192–199, doi: 10.1016/j.ces.2012.02.010.
[20] A. Bhattacharya, V. V. Calmidi, R. L. Mahajan, Thermophysical properties of high porosity metal foams, *International Journal of Heat and Mass Transfer*, 2002, **45**, 1017–1031, doi: 10.1016/S0017-9310(01)00236-4.
[21] G. S. Beavers, E. M. Sparrow, Non-Darcy flow through fibrous porous media, *Journal of Applied Mechanics*, 1969, **36**, 711–714, doi: 10.1115/1.3564773.
[22] L. Friedel, Improved friction pressure drop correlations for horizontal and vertical two-phase pipe flow, *European Two-Phase Group Meeting*, 1979.
[23] W. Zhang, T. Hibiki, K. Mishima, Correlations of two-phase frictional pressure drop and void fraction in mini-channel, *International Journal of Heat and Mass Transfer*, 2010, **53**, 453–465, doi: 10.1016/j.ijheatmasstransfer.2009.09.026.
[24] X. Ji, J. Xu, Experimental study on the two-phase pressure drop in copper foams, *Heat and Mass Transfer*, 2012, **48**, 153–164, doi: 10.1007/s00231-011-0883-4.
[25] H. Hu, Y. Zhu, H. Peng, G. Ding, S. Sun, Effect of tube diameter on pressure drop characteristics of refrigerant–oil mixture flow boiling inside metal-foam filled tubes, *Applied Thermal Engineering*, 2014, **62**, 433–443, doi: 10.1016/j.applthermaleng.2013.09.043.
[26] J. N. Tourvieille, R. Philippe, C. Bellefon, Milli-channel with metal foams under an applied gas–liquid periodic flow: External mass transfer performance and pressure drop, *Chemical Engineering Journal*, 2015, **267**, 332–346, doi: 10.1016/j.cej.2015.01.028.
[27] H. M. Ku, S.-H. Park, J. H. Jeong, Experimental investigation of pressure drop of air-water two-phase flow through open-cell metal foam, *Chemical Engineering Science*, 2021, **241**, doi: 10.1016/j.ces.2021.116701.